Original Research Article

Traumatic brain injury recapitulates developmental changes of axons

Hailong Song [a], Chen Chen [b], Brian Kelley [a], Alexandra Tomasevich [a], Hyoungjoo Lee [c], Jean-Pierre Dolle [a], Jianlin Cheng [b], Benjamin Garcia [c], David F. Meaney [d], Douglas H. Smith [a,*]

[a] Department of Neurosurgery, Center for Brain Injury and Repair, University of Pennsylvania, Philadelphia, PA 19104, United States
[b] Department of Computer Sciences, University of Missouri, Columbia, MO 65211, United States
[c] Department of Biochemistry and Biophysics, Quantitative Proteomics Resource Core, University of Pennsylvania, Philadelphia, PA 19104, United States
[d] Department of Bioengineering, University of Pennsylvania, Philadelphia, PA 19104, United States

ARTICLE INFO

ABSTRACT

During development, half of brain white matter axons are maintained for growth, while the remainder undergo developmental axon degeneration. After traumatic brain injury (TBI), injured axons also appear to follow pathways leading to either degeneration or repair. These observations raise the intriguing, but unexamined possibility that TBI recapitulates developmental axonal programs. Here, we examined axonal changes in the developing brain in young rats and after TBI in adult rat. Multiple shared changes in axonal microtubule (MT) through tubulin post-translational modifications and MT associated proteins (MAPs), tau and MAP6, were found in both development and TBI. Specifically, degenerating axons in both development and TBI underwent phosphorylation of tau and excessive tubulin tyrosination, suggesting MT instability and depolyermization. Conversely, nearby axons without degenerating morphologies, had increased MAP6 expression and maintenance of tubulin acetylation, suggesting enhanced MT stabilization, thereby supporting survival or repair. Quantitative proteomics revealed similar signaling pathways of axon degeneration and growth/repair, including protein clusters and networks. This comparison approach demonstrates how focused evaluation of developmental processes may provide insight into pathways initiated by TBI. In particular, the data suggest that TBI may reawaken dormant axonal programs that direct axons towards either degeneration or growth/repair, supporting further study in this area.

1. Introduction

Early brain development includes exuberant outgrowth of axons, which extend to their nearby targets to establish synapses. Subsequently, as the brain expands in size, the integrated axons are put under tension, resulting in axonal 'stretch growth' (Purohit and Smith, 2016; Smith, 2009). This second phase of axonal growth underlies the development and organization of axons into white matter tracts in the central nervous system (CNS) (Sampaio-Baptista and Johansen-Berg, 2017). Curiously, however, approximately half of the axons are lost during this phase, potentially reflecting a natural process of selection, where some axons are maintained while others undergo developmental axon degeneration (DAD) (Cowan et al., 1984; Luo and O'Leary, 2005; O'Leary et al., 1981; Stanfield et al., 1982; Yang et al., 2013). Although mechanisms of DAD remain largely unknown, it has been shown that the formation of networks during development includes constant

remodeling through cytoskeletal destruction and microtubule (MT) fragmentation (Hoopfer et al., 2006; Luo and O'Leary, 2005; Stanfield et al., 1982), in part through activation of the ubiquitin proteasome system (UPS) (Watts et al., 2003) and semaphorin dependent signaling that eliminate neurites (Bagri et al., 2003).

Interestingly, both axon fragmentation and the UPS are also known to be involved in axon degeneration after traumatic brain injury (TBI) (Johnson et al., 2016; Schweitzer et al., 1993), raising the intriguing possibility that TBI recapitulates some of the axon-clearing processes of ontogeny. Notably, traumatic axon injury (TAI) (also referred to as diffuse axonal injury) is one of the most common pathologies in all severities of TBI and a primary feature of concussion (Johnson et al., 2013; Smith and Meaney, 2000; Smith and Stewart, 2020). In addition, axon degeneration in TAI also appears to follow a selection process since only a subset of axons are lost within each axon tract across the white matter, even in severe TBI (Johnson et al., 2013; Smith and Meaney, 2000).

Potentially, axons that undergo the greatest ultrastructural damage and/or dysfunction are set on a program to degenerate, akin to the presumed selective process of DAD. Conversely, axons that are damaged but do not degenerate after injury, may undergo repair of their cytoskeleton to reinstate structural integrity (Johnson et al., 2013; Pernici et al., 2020), which could potentially harness developmental programs of axon growth. However, axon degeneration and repair in TBI and their related signaling pathways have not previously been examined in context with processes of early development.

Here, we selected peak timepoints of DAD in young rats for comparisons with acute axonal changes after TBI in the adult rats (Bramlett et al., 1997; O'Leary et al., 1981; Povlishock and Christman, 1995; Smith et al., 1997; Stanfield et al., 1982). Focused examination of the cortical and subcortical white matter were performed since these regions have been shown to display the greatest axonal changes (Bramlett et al., 1997; Smith et al., 1997; Stanfield et al., 1982). The aim of this study was to first characterize the axon changes in relation to the regulation of MT stability in both development and after TBI. Specifically, we examined modulations of tubulin post-translational modifications (PTMs) and MT associated proteins (MAPs) (Baas et al., 2016; Janke and Magiera, 2020). We then identified the extent of shared proteome changes and associated signaling pathways that involve and potentially govern axon growth/repair and degeneration processes.

2. Material and methods

2.1. Experimental design and animals

A total of fifty-four male Sprague-Dawley (Charles River) rats were used and housed with a 12-hour light/dark cycle and given unrestricted access to food and water. Specifically, for DAD study, rats at postnatal day 5 (P5), P14, P21, and naïve adult (4 months) were included since this time span includes the greatest loss of axons (O'Leary et al., 1981; Stanfield et al., 1982). As for TBI study, adult rats with TBI induced by lateral fluid percussion injury (FPI) at 24 h post injury (also a peak timepoint of marked axon degeneration) (Bramlett et al., 1997; Povlishock and Christman, 1995) and sham control were incorporated. Male animals, especially at early postnatal days, were identified by the presence of striated testes found below the kidneys, as previously described (Dolle et al., 2018). Numbers of animals used for proteomics/Western blot (WB) and immunohistochemistry (IHC) were specified in Table 1.

Data-independent acquisition-based liquid chromatography with tandem mass spectrometry (LC-MS/MS) experiments were carried out to independently characterize the proteomic changes during both development and following TBI (Fig. 4A). All experimental analyses were treated in a double-blinded manner. All animal procedures were performed in accordance with the National Institutes of Health guide for the care and use of laboratory animals and protocols were approved by the Institutional Animal Care and Use Committee at the University of Pennsylvania.

2.2. Lateral FPI model

Adult Sprague-Dawley rats (4 months old, 480 ± 30 g) were subjected to a 'mild' (average 2.01 atm with a range from 1.89 to 2.22 atm) lateral FPI or sham injury, as previously described (Clausen et al., 2019; Koch et al., 2020; Smith et al., 1997). Notably, the 'mild' designation of these injury parameters reflects the absence of overt post-injury pathologies such as contusion or hemorrhage and the model includes rapid recovery to typical ambulatory, grooming and feeding behavior, without apnea or seizure at the time of impact (Fig. S1A). This Lateral FPI model led to predominant TAI in both cortex and subcortical white matter. Briefly, animals were anesthetized with isoflurane (1–5%) and a 5 mm craniotomy was performed over the right cortex 4 mm lateral to the midline (as marked between lambda and bregma). A plastic female Luer-Lok disc was used to secure the craniotomy site and attached to the fluid percussion device filled with sterile saline for initiating the injury. After injury, animals were released from anesthesia, returned to their cages, and observed until fully awake. All animals survived after this experimental procedure, prior to sacrifice. The rats were sacrificed at 24 h after lateral FPI, when extensive axonal injuries were expected (Koch et al., 2020; Pierce et al., 1996). Sham-injured animals received identical treatment without FPI. Following TBI, injured rats had an average righting time of 398 s post-injury, compared to the average of 29 s for the sham animals. Animals' behavioral outcomes at 24 h post injury were evaluated using the modified neurological severity score (mNSS) (Li et al., 2000), by assessing the motor, placing, movement, sensory, and reflex functions. The animals at 24 h post injury had an average mNSS score of ~1.64 without overt contusion or change in weight, altogether suggesting a 'mild' injury (Fig. S1B-D).

2.3. Tissue extraction and preparation

For fixed tissue preparation, animals were sacrificed under deep anesthetization using ketamine/xylazine mixture followed by perfusion with cold saline and 10% neutral buffered formalin. After brain extraction with 24 h post fixation, the samples were blocked into 2 mm thick coronal sections and processed for standard paraffin embedding in an automated tissue processor (Shandon Scientific Instruments, Pittsburgh, PA) (Johnson et al., 2016). Serial sections (8 μm) were cut on a Leitz rotary microtome (Leica, Malvern, PA).

For fresh tissue preparation, cerebral cortices with subcortical white matter were dissected from the immediately euthanized rat brains as previously described (Song et al., 2019a, 2019b). Since axonal changes during development and after TBI are most prominent in cortical and subcortical white matter (Bramlett et al., 1997; Smith et al., 1997; Stanfield et al., 1982), these regions were selected to examine potentially related molecular changes associated with both processes (Fig. 4A). Tissue lysates from right cortex were sonicated on ice in RIPA sample buffer (ab156034 Abcam, Cambridge, UK) with protease inhibitor cocktail (P8304 Sigma-Aldrich, 1:100) and PMSF (100 μM) added. Tissue homogenates were then centrifuged at 12,000g, for 20 min at 4 °C. The supernatant was then transferred for protein concentration measurement by BCA assay (Thermo Fisher Scientific, Waltham, MA) followed by adding 4x Laemmli sample buffer (Bio-Rad, Hercules, CA) and denaturing at 95 °C for 5 min.

2.4. Data-independent acquisition sample preparation

Brain tissue was freshly extracted as described above and homogenized in lysis buffer containing 5% SDS, 100 mM NH_4HCO_3, pH 8.0, and 1x proteinase inhibitor cocktail (HALT, Thermo Fisher Scientific, Grand Island, NY). The lysate was sonicated on ice for 1 min with two-second pulses every 30 s. Insoluble debris was pelleted by centrifugation at 13,500 rpm for 30 min at 4 °C, and the supernatant was stored in aliquots at 4 °C. Protein concentrations were determined with the Bradford assay using bovine serum albumin as a standard. Denaturation /

Table 1
Experimental design and animal usage.

Study	Animal grouping	Number of animals used for (n)		
		Proteomics	WB	IHC
Development	P5	3		4
	P14	3		4
	P21	3		4
	Naïve adult	3		4
TBI	TBI adult	3	6	5
	Sham adult	3	4	5

reduction of 100 μg of each sample was performed by adding 20 mM dithiothreitol over 60 min at 52 °C. The solution was stored at room temperature in 50 mM iodoacetamide in the dark for 60 min. Trypsin digestion was performed as described in the manufacture's protocol of the S-Trap micro-Spin column (PROTIFI, Farmingdale, NY) (HaileMariam et al., 2018). After tryptic digestion, the peptide mixture was desalted with the C18 micro spin column (C18, Harvard Apparatus, Holliston, MA). The column was washed with 200 μl of 100% acetonitrile and equilibrated with 200 μl of loading buffer (0.1% formic acid). Peptides were loaded onto the column, washed with a loading buffer and eluted with 200 μl of 70% acetonitrile / 0.1% formic acid. All steps for loading, washing, and elution were carried out with benchtop centrifugation (300g for 2 min). The eluted samples were dried in a centrifugal vacuum concentrator, reconstituted with 0.1% formic acid. 2 μg of each sample was injected into LC-MS/MS.

2.5. Data-independent acquisition and processing

Peptides were analyzed on a Q-Exactive HFX (Thermo Scientific) attached to an UltiMate™ 3000 RSLCnano System (Thermo Scientific). Mobile phase A for LC separation consisted of 0.1% formic acid in deionized water, and mobile phase B consisted of 0.1% formic acid in 80% acetonitrile (ACN). Peptides were eluted with a 97 min gradient from 1% to 25% ACN, to 45% ACN (24 min), to 95% ACN (0.5 min) and to 95% ACN (10 min), to 1% (0.5 min) and 1% ACN (10 min). All DIA analysis was done described previously (Searle et al., 2018). Briefly, for each chromatogram library, six chromatogram library acquisitions with DIA spectra were acquired with a 4 mass/charge ratio (m/z) precursor isolation window at 30 K resolution, 1e6 automatic gain control (AGC) target 60 ms maximum injection time using an overlapping window (396.43–502.48, 496.48–602.52, 596.52–702.57, 696.57–802.61, 796.61–902.66, and 896.6–1002.70 m/z) (Searle et al., 2018). For quantitative samples, DIA spectra were acquired with an 8 m/z precursor isolation window at 15 K resolution, 1e6 AGC target, 20 ms maximum injection time, and 75 loop count using an overlapping window pattern from 388.43 to 1012.70 m/z using window (Fig. 4A).

2.6. Protein identification and quantitation

EncyclopeDIA program (version 0.9.0) was used for protein identification and quantification (Searle et al., 2018). Thermo RAW files were converted to mzML format using the ProteoWizard package. The EncyclopeDIA was configured with default settings (10 ppm precursor, fragment, and library tolerances, considering both B and Y ions, and trypsin digestion were assumed). The MS measured peptide levels were consistent throughout all biological replicates and the data quality was further validated by high reproducibility among replicates in the clustering analysis (Fig. S2).

3. IHC staining

IHC was carried out as previously described (Johnson et al., 2016), and allowed to examine axon and related molecular changes in both cortex and subcortical white matter. Serial tissue blocks from ~Bregma − 1.30 mm to − 3.30 mm were stereologically cut and surveyed. Sections (8 μm thick) were first deparaffinized at 60 ℃ and rehydrated through exchanges of xylene, 100%, 95% ethyl alcohol, and distilled water. Aqueous hydrogen peroxide was used to quench endogenous peroxidase activity for 15 min. Antigen retrieval was then carried out by microwaving in Tris EDTA buffer (pH 8.0) in a pressure cooker. Next, slides were blocked using 1% normal horse serum (Vector Labs, Burlingame, CA, USA) in Optimax buffer (BioGenex, San Ramon, CA, USA) for 30 min at room temperature (RT). Overnight incubation with primary antibodies, including AT8 (MN1020 Thermo Fisher Scientific, 1:2000), amyloid precursor protein (APP) (22c11 MAB348 Millipore, 1:130,000), Iba1 (019–19741 Wako, 1:10,000), acetylated tubulin

(Ace-Tub) (T7451 Sigma-Aldrich, 1:10,000), tyrosinated tubulin (Tyr-Tub) (T9028 Sigma-Aldrich, 1: 2000), and polyglutamylated tubulin (PolyGlu-Tub) (T9822 Sigma-Aldrich, 1:2000), were performed at 4 °C in a humidified chamber. The sections were further probed with the corresponding biotinylated secondary antibodies (1:250, Vectastain Universal Elite kit, Vector Labs, Burlingame, CA, USA) for 30 min at RT following by an avidin biotin complex (ABC) and 3,3′-Diaminobenzidine (DAB) peroxidase substrate application as per the manufacturer's protocols. Hematoxylin counterstain was used and sections were finally examined under light microscopy on a Nikon Eclipse 80i platform (Nikon, Tokyo, Japan).

3.1. Immunofluorescent (IF) staining and quantitative analysis

Immunofluorescent staining and imaging were performed as previously described (Johnson et al., 2016). Tissue sections were processed consistent with the IHC protocol specified above, with the omission of the hydrogen peroxide step. Primary antibodies, including APP (512700 Invitrogen, 1:500), AT8 (1:2000), Ace-Tub (1:1000), Tyr-Tub (1:1000), detyrosinated tubulin (DeTyr-Tub) (AB3201 Millipore, 1:500), PolyGlu-Tub (1:500), and MAP6 (from Dr. Annie Andrieux, 1:2000), were incubated overnight. Sections were then probed with corresponding fluorophore-conjugated donkey anti-mouse 647 and donkey anti-rabbit 488 secondary antibodies (1:250, Invitrogen, San Diego, CA) for 60 min. Coverslips were mounted with sections immersed in VEC-TASHIELD Vibrance antifade mounting medium with DAPI (Vector Labs, Burlingame, CA, USA). Fluorescence photomicrographs of the areas of interest were captured using a Leica DM6000 microscope. For IF quantification, APP staining was used to mark APP positive (+) or APP negative (-) axons. The intensity of MAP6 was measured using ImageJ software. The mean value from each rat was further compiled for statistical analysis.

3.2. WB analysis

Protein samples (15 μg) were added to 4x SDS sample buffer with 1% 2-mercaptoethanol and resolved on 4–15%, 1.5 mm SDS-PAGE gels as previously described (Song et al., 2019a, 2019b). Proteins were then transferred to a nitrocellulose membrane. The membrane was first incubated in tris-buffered saline plus 0.1% Tween-20 (TBST) containing 5% non-fat milk or 5% bovine serum albumin for 1 h at RT and then incubated with primary antibodies, including SMI312 (837904 Biolegend, 1:1000), APP (512700 Invitrogen, 1:1000), βIII-tubulin (T9578 Sigma-Aldrich, 1:4000), Iba1 (1:1000), AT8 (1:1000), Tau5 (577801 Millipore, 1:5000), MAP6 (from Dr. Annie Andrieux, 1:5000), α-tubulin (B512 Sigma-Aldrich, 1:5000), Acetyl-Tub (1:10,000), DeTyr-Tub (1:500), Tyr-Tub (1:1000), PolyGlu-Tub (1:1000), and actin (A5441 Sigma-Aldrich, 1:5000) at 4 °C overnight. The membrane was incubated with corresponding secondary antibodies (1:10,000, IRDye, LiCor) for 1 h at RT. Immuno-reactive bands were detected using the LiCor imaging system. Naïve adult and sham control animals were pooled as "N/S Adult" for further WB quantification due to no major protein expression difference, such as α-tubulin and MAP6, observed in between (Fig. S3). Normalization against "N/S Adult" was used to quantify and compare relative protein expression ratio in different groups.

3.3. Bioinformatics and statistical analysis

The general bioinformatics analysis was performed as previously described (Song et al., 2019a, 2019b). Specifically, Welch's test and t-distribution were performed with R function "t.test". The heatmap was generated using R package "pheatmap". Principal Component Analysis (PCA) plot was generated using R package "prcomp" and the first two components (PC1 and PC2) were plotted using R package "rgl". Pathway and gene ontology (GO) enrichment analyses were performed using R package "clusterProfiler". GO was used to interpret the functional

profiles of sets of proteins using established system of classification (The Gene Ontology, 2019). Differentially expressed proteins were further enriched with Kyoto Encyclopedia of Genes and Genomes (KEGG) pathway database with function "enrichKEGG", and cellular component enrichment analysis was performed with function "enrichGO". The Reactome enrichment analysis was performed with R package ReactomePA. All cutoffs for p value were set to 0.05 for enrichment analysis.

Weighted gene correlation network analyses (WGCNA) is a system biology and data processing method for describing biological networks based upon correlations among variables (Langfelder and Horvath, 2008). Here it was applied to identify clusters (modules) of highly correlated co-expressed proteins. Briefly, R package WGCNA is used to generate the gene clusters. We chose unsigned Topology Overlap Matrix with soft-thresholding power for network construction set to 6. After the gene clusters were generated, we performed PCA for each of the clusters and the first principal component was extracted as the Module Eigengene (ME). Pearson correlation was used as previously described to calculate the goodness of fit (Bai et al., 2020), and the proteins assigned to the most correlated clusters was considered with a cutoff of R at least 0.5.

Further, machine learning-based bioinformatic analysis was performed using QIAGEN's Ingenuity Pathway Analysis (IPA, QIAGEN Redwood City) (Song et al., 2019a, 2019b). This was used to examine canonical pathways, upstream transcriptional regulators, functional networks, and protein-protein interaction networks. Changes in protein expression relevant to these functional networks were further selected and compared between development and after TBI based on shared patterns. Other statistical analyses were performed using GraphPad Prism statistical software (GraphPad Software Inc. La Jolla, CA). One-way analysis of variance (ANOVA) followed by Tukey post-hoc multiple comparison and unpaired student's t-test were used to determine differences between groups. All data were expressed as means $\pm$ SEM. Differences were considered significant at $p < 0.05$ for all analyses, with * indicating $p < 0.05$; ** $p < 0.01$; *** $p < 0.001$; **** $p < 0.0001$. All of the original proteomic data and bioinformatic processing can be accessed through Synapse: https://www.synapse.org/#!Synapse: syn22267275/wiki/; username: hailong_proteomics; password: proteomics2020).

4. Results

4.1. Changes in axon and MT stability between development and after TBI

To examine the axon changes, we first focused on axon degeneration processes by examination of APP IHC. In TAI, hallmark axonal swellings have been shown to be linked to mechanical damage to axonal MTs and subsequent interruption of axonal transport. Due to its abundant concentration in axons, APP immunostaining is the 'gold standard' technique to identify these post-TAI axonal swellings (Gentleman et al., 1993). Notably, the mechanical origin of these morphological changes in TAI represents an obvious difference from events that initiate axonal degeneration in development. Accordingly, we evaluated differences and similarities of APP changes in TAI and development. Interestingly, protein levels of APP were significantly elevated during development at P14 and P21, but unchanged after TBI (Fig. 1**A**). Only sparse APP+ swollen axonal profiles were observed during development, suggesting that overt axon swelling is not a prominent feature of axon degeneration during development. This was not surprising, since mechanical damage to microtubules and resulting protein transport interruption seen in TBI does not occur in development. However, after TBI in the present study, characteristic APP+ swollen axonal profiles were observed across the white matter and beyond, typically in the form of various swellings at periodic intervals along individual axons, but also as terminal bulbs of disconnected axons (Fig. 1**B**). Although abundant large axonal swellings appeared predominantly after TBI, both TBI and development displayed

activated microglia throughout the white matter, with characteristic ameboid/bushy morphologies (Fig. S4C-**D**).

Despite the overt differences in the initiation of axonal degeneration and morphological character in early development and after TBI, there also appeared to be multiple similarities between TAI and DAD, suggesting shared pathways. Most notably, mechanisms regulating functional stability of MT through tubulin PTMs were commonly found in development and after TBI, particularly involved with acetylation (Acetyl-Tub), polyglutamylation (PolyGlu-Tub), and tyrosination/detyrosination (Tyr-Tub and DeTyr-Tub) (Moutin et al., 2021). Specifically, reduction of Acetyl-Tub levels as well as elevations of PolyGlu-Tub and Tyr/DeTyr-Tub dependent changes (ratio) were consistently identified during development (especially at P5) and after TBI (Fig. 1C-D). Concurrently, levels of total α-tubulin were significantly reduced ($\sim$14%) from early development through adulthood, suggesting pruning of neurites through DAD, in contrast to a more modest decrease after TBI. IHC staining supported the WB results and showed the selective immunoreactivity in axons (Fig. S5).

While similar global tubulin PTMs changes in brain were demonstrated, the functional mechanisms of each PTM profile acting on individual axon and its relationship to axon degeneration or growth/repair remain unclear. Previous studies suggest that tyrosination occurrs only on soluble tubulin, while acetylation and polyglutamylation specifically interacts with tubulin that has already been polymerized in MTs (presenting as stable MTs) (Song and Brady, 2015). Intriguingly, the present results demonstrated that APP+ axons only showed excessive tubulin tyrosination, reflecting MT instability and depolyermization associated with axon degeneration (Fig. 1**G**). Certain axonal swelling/beading were also associated with increased cytosolic Tyr-Tub expression. Conversely, other nearby axons that did not demonstrate APP+ swellings maintained tubulin acetylation and polyglutamylation staining, which correlated with MT stability and potentially promote axon growth/repair (Fig. 1**E-F**). Overall, the current data suggests that tubulin PTMs could contribute to pathways associated with both developmental and TBI related changes of axons.

4.2. Changes in axon MAPs expressions between development and TBI

In addition to tubulin PTMs, axon MT stability can also be modulated by the expression and binding of MAPs, especially tau and MAP6 that are both highly enriched selectively in axons. During development, levels of total tau increased ($\sim$33%) from P5 to P21 and gradually decreased ($\sim$29%) toward adulthood. This may reflect selective loss unwanted axons during DAD via changes in MT stability (Fig. 2**A**). Indeed, increased soluble tau phosphorylation (p-tau) (at Ser202/Thr205) was particularly evident at P5 and P14 with an axonal thread pattern in cortex (Fig. 2**A-B**). Interestingly, p-tau+ axons were not found colocalized with DeTyr-Tub profiles (MT stabilization), suggesting that increases in p-tau could account for a loss of MT stabilization, which could push the axons towards a degeneration pathway (Fig. 3**A**).

In contrast to tau, the levels of total MAP6 and especially its neuronal form (MAP6-N) were lower than adults (Fig. 2**C-E**), with MAP6-E (embryonic isoforms) transiently increased from P5 to P14 (32%). Notably, MAP6–70kD (function has not yet been characterized) showed a trend similar to MAP6-N. Such changes together suggest a gradual shifting of expression between tau and MAP6 in axons during development. Further, MAP6 expression strongly co-localized with Acetyl-Tub, but not Try-Tub, suggesting its potential supportive role for MTs stabilization and axon growth/repair (Fig. 3**B-C**).

Importantly, these changes in MAPs during development were similar to those found after TBI. Specifically, increases in p-tau expression were identified at 24 h post injury. Distinctively, unlike axonal tread pattern in development, TBI caused p-tau depositions in neuronal cell body and axons with grain-like profiles (Fig. 2**B**). Clusters of granular-like p-tau profiles could also be observed within white matter. Such dense and localized aggregation acutely after TBI implied axonal
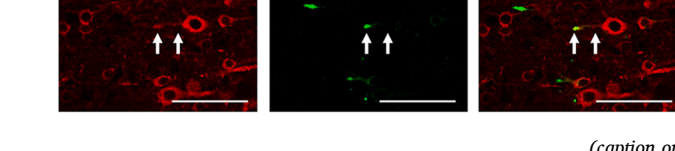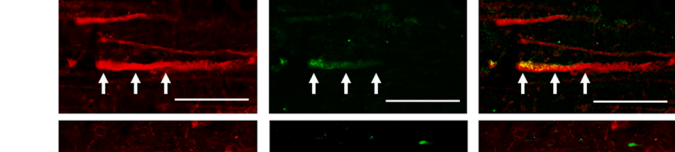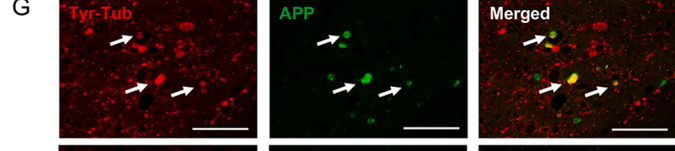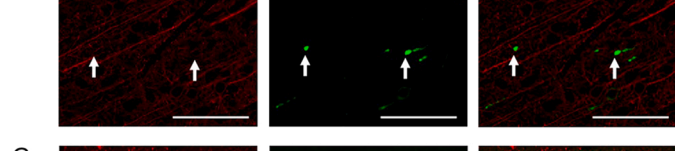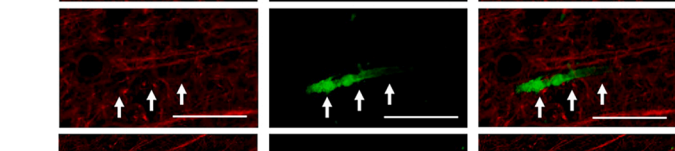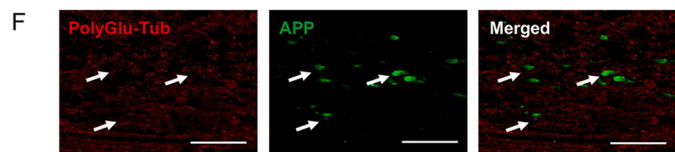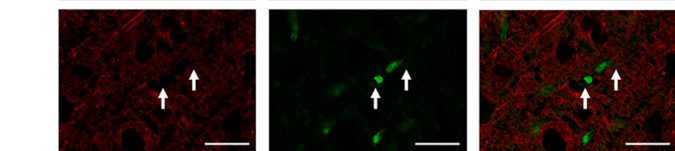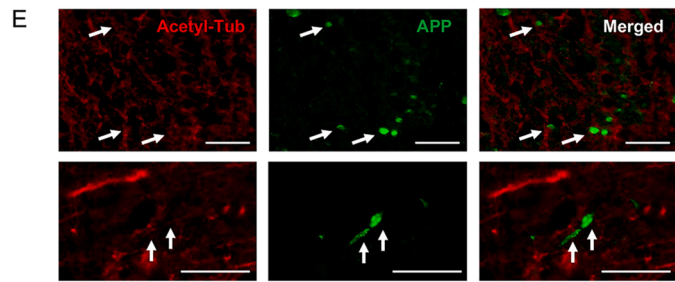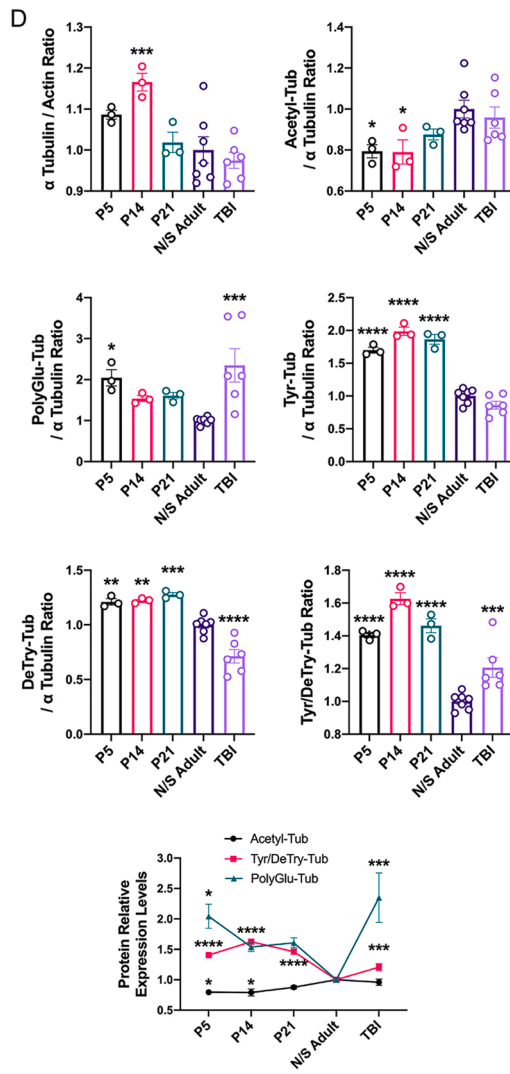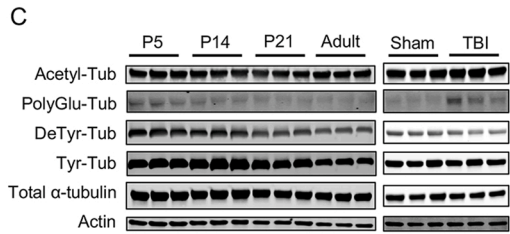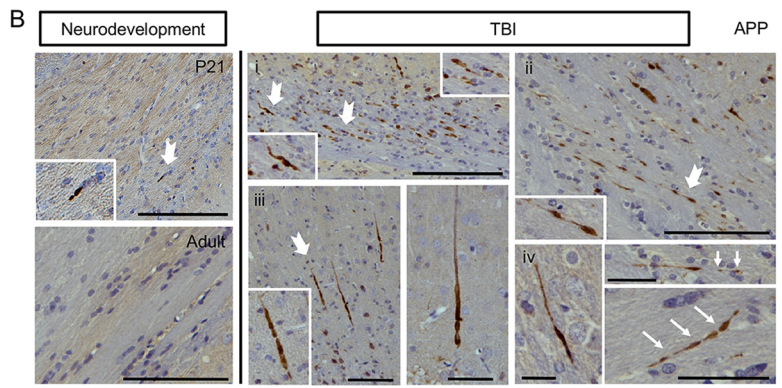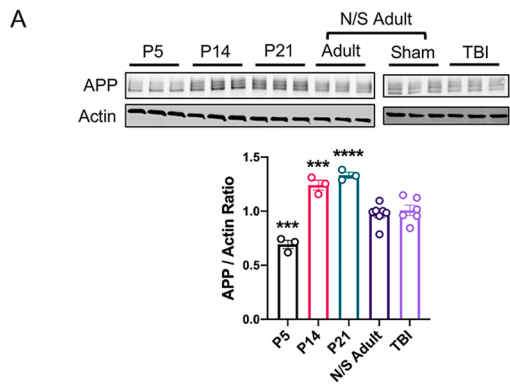
(caption on next page)

Fig. 1. Axon degeneration changes and tubulin PTMs. (A) Western blot analysis of APP (110–130 kD) and actin (42 kD) were shown. Naïve adult and sham control animals were pooled as "N/S Adult" for further WB quantification due to no major protein expression difference between the two groups. (B) APP IHC stainings were compared between DAD and TBI. During DAD, sporadic profile of APP staining was captured in the white matter (corpus callosum) (scale bar = 100 μm), with no APP staining identified in naïve adult or sham control animals (scale bar = 50 μm). In contrast, extensive APP accumulations were observed after TBI. i-ii) Various forms of white matter (corpus callosum and external capsule) APP positive swellings were observed, including terminal swelling and beading (white notched arrows indicated the enlarged regions shown in the insets) (scale bar = 100 μm (i) and 50 μm (ii)). iii) Focal APP pathologies were observed in the cortical area relevant to the FPI injury (scale bar = 50 μm (left) and 25 μm (right)). iv) APP fusiform accumulations were also seen in white matter (white arrows pointed to beadings in adjacent to large swellings suggesting of axonal transport interruption) (scale bar = 10 μm (left) and 25 μm (right)). (C) WB analysis of tubulin PTMs were shown. (D) Quantitative comparisons of total α-tubulin, Acetyl-Tub, PolyGlu-Tub, Tyr-Tub, DeTyr-Tub, and Tyr/DeTyr-Tub expressions were measured. (E-G) IF staining of Acetyl-Tub (red) and APP (green) were shown (scale bar = 25 μm). White arrows pointed to APP positive swollen axonal profiles with no obvious Acetyl-Tub expression observed. The upper panel represented subcortical white matter region, while the rests showed cortical staining. (F) Similarly, PolyGlu-Tub (red) and APP (green) IF staining were shown (scale bar = 50 μm). (G) IF staining of Tyr-Tub (red) and APP (green) were shown (scale bar = 50 μm). White arrows pointed to co-localizations of Tyr-Tub and APP positive swollen axonal profiles. Again, the upper panel represented subcortical white matter region, while the rests showed cortical staining.
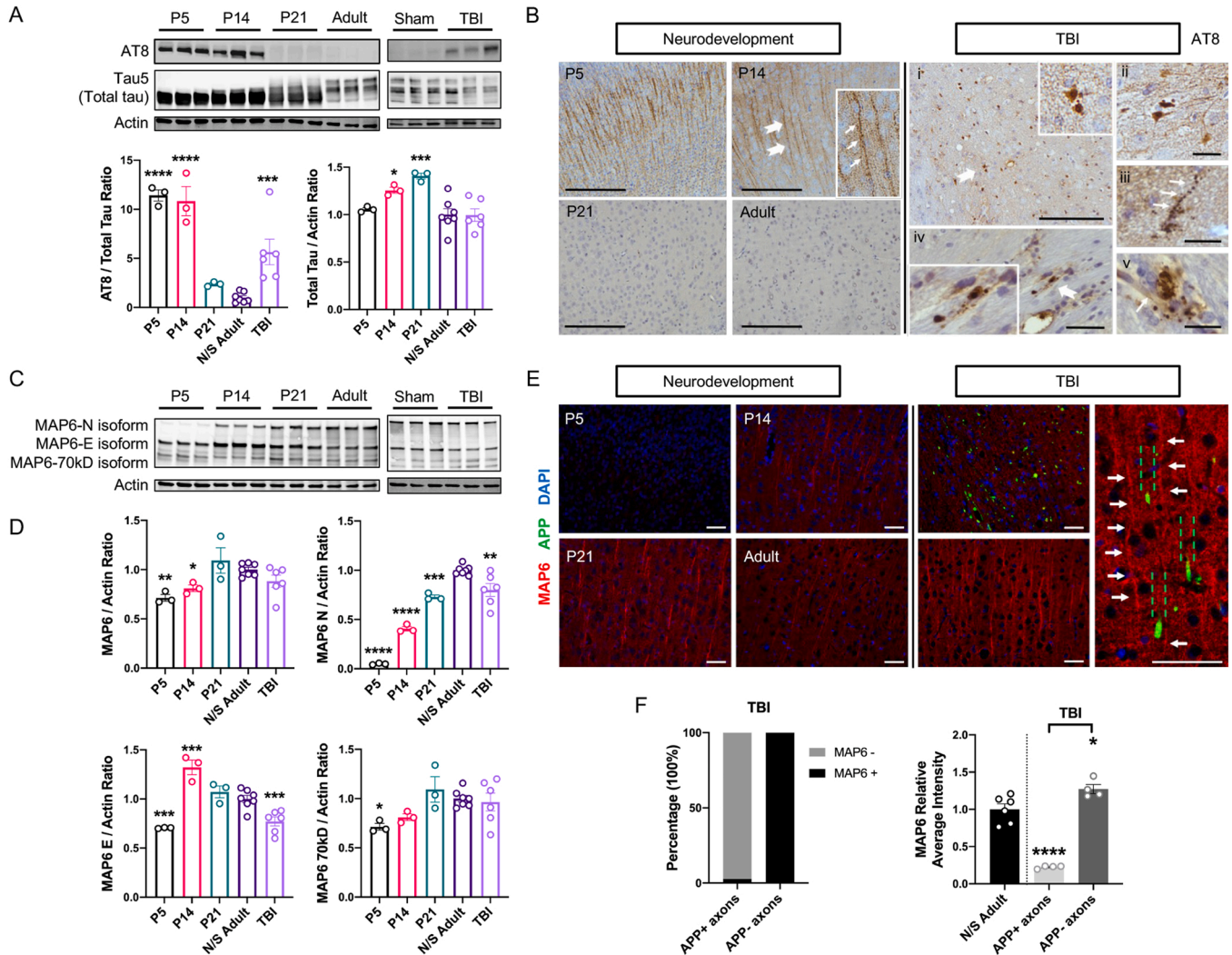
Fig. 2. Changes in tau and MAP6 expressions during development and after TBI. (A) Western blot analysis of soluble phosphorylated tau (~60kD), total tau (Tau5) (45–68kD), and actin (42kD) were shown. (B) AT8 IHC stainings were compared between DAD and TBI. Widespread phosphorylated tau at Ser202/Thr205 were captured in cortex during DAD (white notched arrows indicate the enlarged regions shown in the insets, scale bar = 100 μm). i-v) Focal and sparse AT8 stained phosphorylated tau depositions in the cell body from the ipsilateral cortical area were captured at 24 h post TBI (i, white arrowhead indicated the enlarged regions shown in the insets, scale bar = 100 μm; ii, scale bar= 25 μm). Grain-like (small round) profiles were also observed (iii, white arrows pointed to a few AT8 positive profiles likely along the axon, scale bar = 10 μm). AT8 swollen profiles (dense granular like) were shown in the white matter (corpus callosum and external capsule) as well (lower panels, scale bar = 25 μm (iv) and 10 μm (v)). (C-D) Western bot analysis of MAP6 and actin were shown. Different MAP6 isoforms were marked as MAP6-N (neuronal) isoform at ~125kD, MAP6-E (embryonic) isoform at ~90kD, and MAP6–70kD isoform at ~70kD. (E) IF staining of MAP6 (red) and APP (green) profiles compared between development and TBI were shown (scale bar = 50 μm). (F) The percentage of MAP6 expressions and relative intensities were compared between control and TBI animals (separating APP positive vs negative axons).
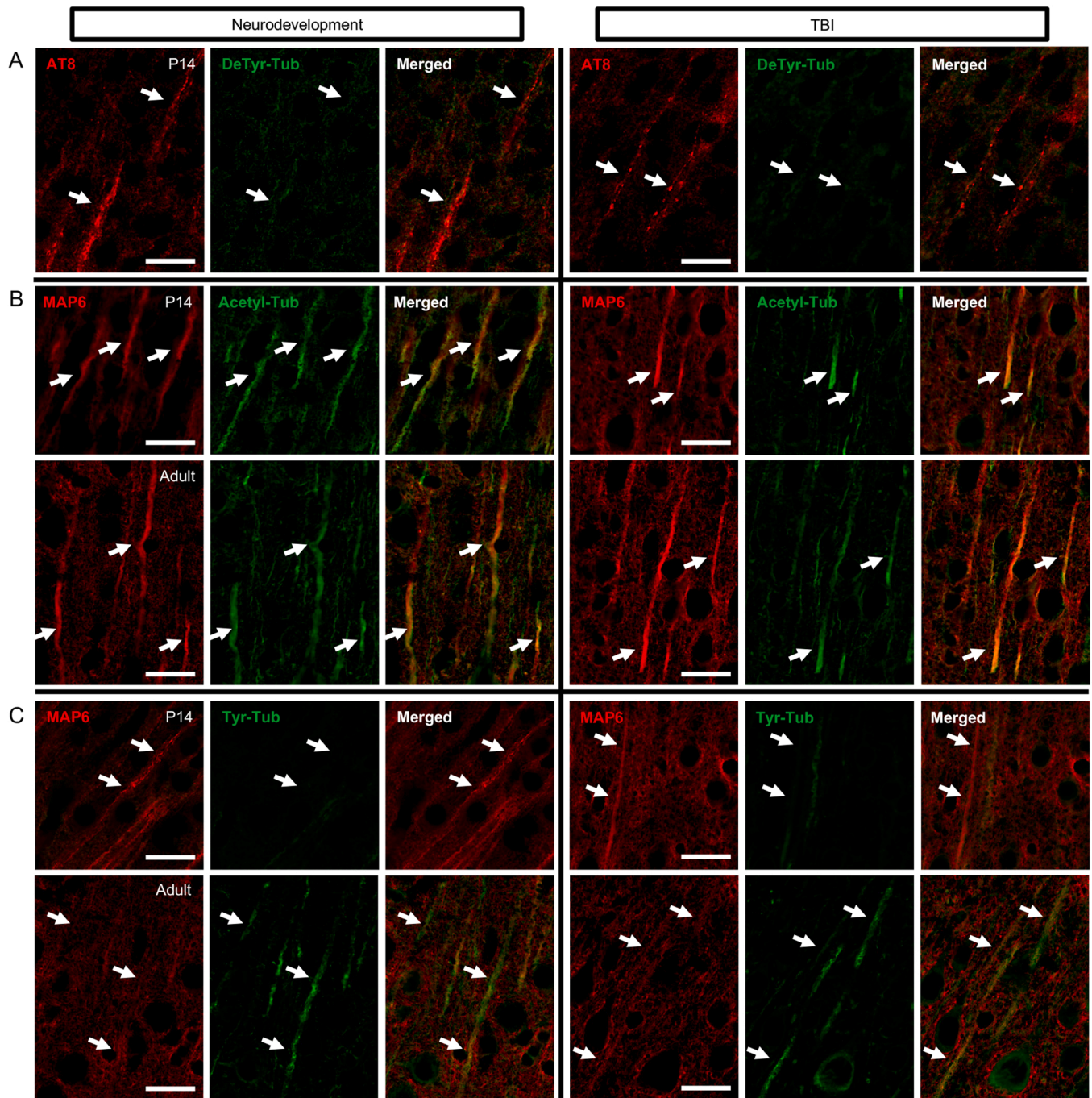
Fig. 3. IF co-localization between tau, MAP6 and different tubulin PTMs during development and after TBI. (A) IF staining showed no obvious AT8 (red) and DeTyr-Tub (green) co-localization (scale bar = 25 μm). (Other tubulin PTM markers, including Tyr-Tub antibodies, are from the same source as p-tau. Therefore, a directly co-localization with those markers is unable to achieve). (B) IF staining showed evident co-localization between MAP6 (red) and Acetyl-Tub (green) (scale bar = 25 μm). (C) IF staining showed no obvious MAP6 (red) and Tyr-Tub (green) co-localization (scale bar = 25 μm).

transport disruption that was not seen during development. Similarly, p-tau was not found co-localized with DeTyr-Tub (presenting as stable MTs), suggesting an association of p-tau with MT instability (Fig. 3A). Overall, the presence of p-tau for both development and TBI appears to be associated with axon degeneration.

Intriguingly, after TBI, only a slight reduction of total MAP6 was identified, with significant changes in both MAP6-N and MAP6-E iso-forms (Fig. 2C-D). Noteworthy, such loss of MAP6 profiles were evident in those APP+ axons (in both cortex and subcortical white matter), potentially leading to degeneration (Fig. 2E). However, other nearby axons (without APP+ profiles) showed significantly increases in MAP6

expressions (Fig. 2F). These axons were co-localized with Acetyl-Tub, but not Try-Tub, which is suggestive of an association with MT stabilization that would promote axon repair (Fig. 3B-C).

4.2.1. Global proteome dynamics and signaling pathway involvement during development and after TBI

With the observations that both development and TBI induced changes in axons associated with regulation of MT stability that may direct axons towards either growth/repair or degeneration, we examined the systematic molecular changes and signaling pathways under both conditions utilizing data-independent acquisition-based LC-MS/MS
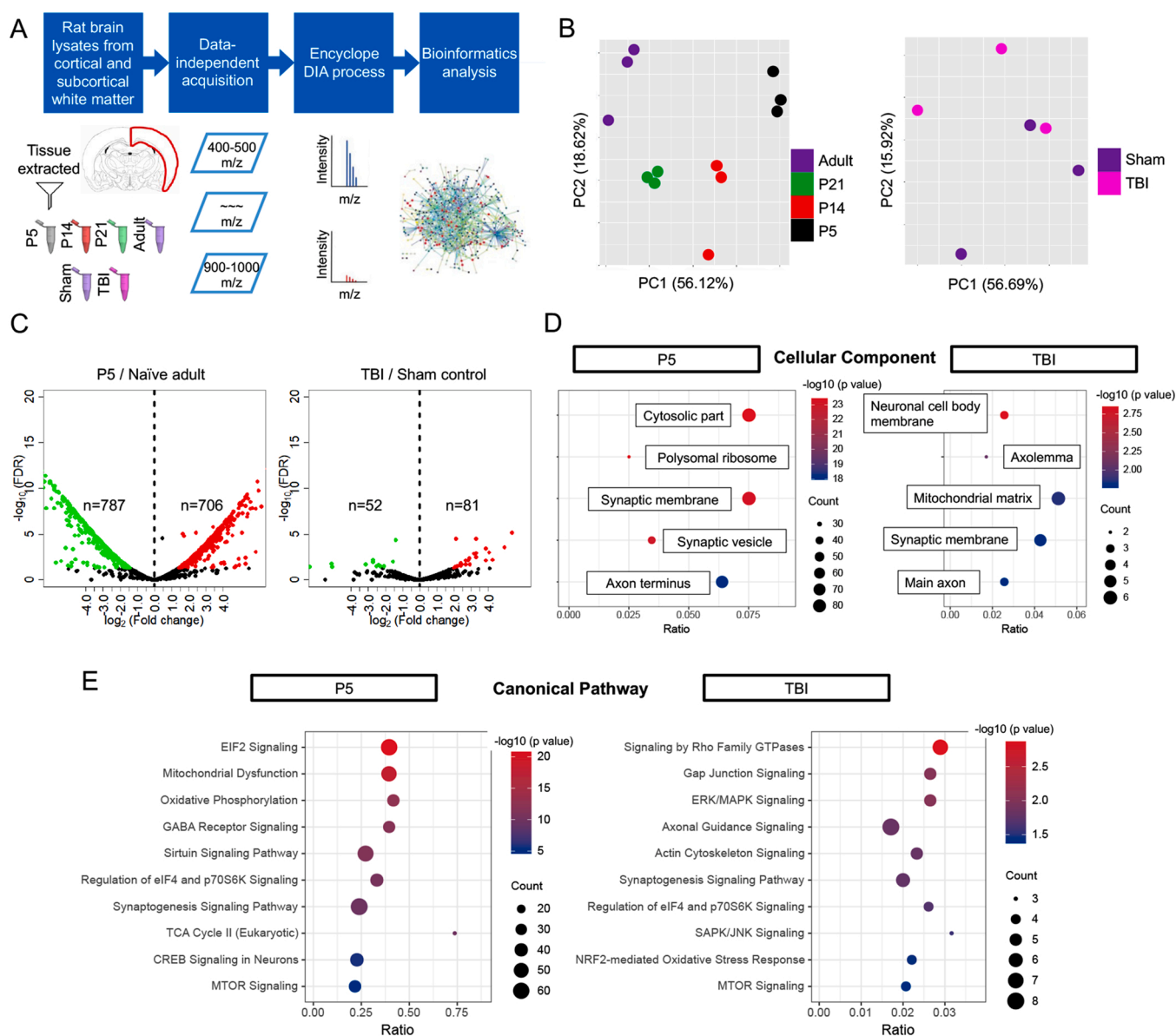
Fig. 4. Global protein expressions and biological annotations during development and after TBI. (A) Data-independent acquisition (DIA)-based LC-MS/MS quantitative proteomics workflow. (B) PCA analyses showed clear separation of differentially expressed proteins among various groups. (C) Volcano plots showed the distribution of all proteins identified and compared between P5 and TBI. Dashed lines indicated the thresholds of log2 (Fold change). Red, green, and black dots represented upregulated, downregulated, and unchanged protein, respectively. Numbers of differentially expressed proteins were marked as n. (D) Major cellular components identified and compared between P5 and TBI. The length of the bar represented the significance of each GO enrichment (-log10 (p value)), and the size of the circle represented the total numbers of proteins enriched. (E) Top canonical pathways enriched and compared between P5 and TBI. The canonical pathways were ranked based on the -log10 (p value), and the size of the circle represented the total numbers of proteins enriched.

(Fig. 4A). A total of 28,294 peptides were probed leading to the identification of 3244 proteins during development, and 22,356 peptides with 2836 proteins following TBI, respectively (Table S1 and S2). The overall proteome expressions diverged across different neurodevelopmental stages (with PC1 of 56% and PC2 of 19%) and following TBI (with PC1 of 57% and PC2 of 16%) as visualized by the PCA plot (Fig. 4B and Table S3). Collectively, there were a total of 1493, 675, 173, and 133 differentially expressed proteins identified at P5, P14, P21, and after TBI, as compared to either naïve adult or sham control groups in each independent dataset (Fig. 4C). Indeed, P5 yielded the largest numbers of differentially expressed proteins, with a significant portion (n = 858, 57.5%) distinctively up- or down-regulated, reflecting a battery of molecular activities during early development.

To study the biological relevance of the characterized proteome changes under both TBI and development, knowledgebase of GO, KEGG,

Reactome, and machine learning-based IPA were systematically queried to annotate protein enrichments. During development, top biological processes were identified particularly at P5, some of which were transmembrane transport, ATP metabolic process, synaptic signaling, cell-cell signaling, and establishment of localization. After TBI, the top biological processes were recognized as glutamate receptor signaling pathway, system process, synaptic signaling, cytosolic calcium ion transport, and nervous system processes.

Since global proteome changes were observed in mixed cellular compartments, cellular component analysis was further conducted. Interestingly, similar axonal cellular component enrichments were captured both during development (P5: synaptic membrane, synaptic vesicle, and axon terminus. P14: synaptic vesicle, distal axon, and axon terminus; P21: myelin sheath, perikaryon, and axon terminus) and after TBI (axolemma, synaptic membrane, and main axon) (Fig. 4D and

Canonical pathway analysis was further used to understand the signaling cascades regulating development and changes after TBI. As expected, both axon growth and DAD processes were reflected during development with enrichments of EIF2 signaling (implicated in local axon translation (Cagnetta et al., 2019)), oxidative phosphorylation (related to axon development and degeneration (Smith and Gallo, 2018)), sirtuin signaling pathway (involved in axonogenesis, axon elongation, and axon survival (Li et al., 2013)), synaptogenesis signaling pathways, and regulation of eIF4/p70S6K and mTOR signaling (protein translational regulation) (Fig. 4E and Table S4). Such pathways were regulated by key upstream transcriptional regulators, including sirtuin 2

(modulate histone and α-tubulin, p value=5.51E-06), shank3 (control actin cytoskeleton, 3.39E-05), and maf (interact with ARE mediated transcription, 1.29E-04).

In contrast, after TBI, Rho family GTPases signaling (regulating intracellular cytoskeletal and facilitating axonal morphological changes (Hall and Lalli, 2010)), axonal guidance, SAPK/JNK, and actin cytoskeleton signaling were captured, possibly reflecting both axon repair and degeneration processes. Distinct upstream regulators, including histone h4 (modify histone, 1.72E-03), CREBBP (enhance transcriptional activity of cAMP-responsive genes, 7.05E-03), and PPARA (regulate lipid oxidation, 4.88E-03), were involved as opposed to development. Nonetheless, common pathways that played an role in
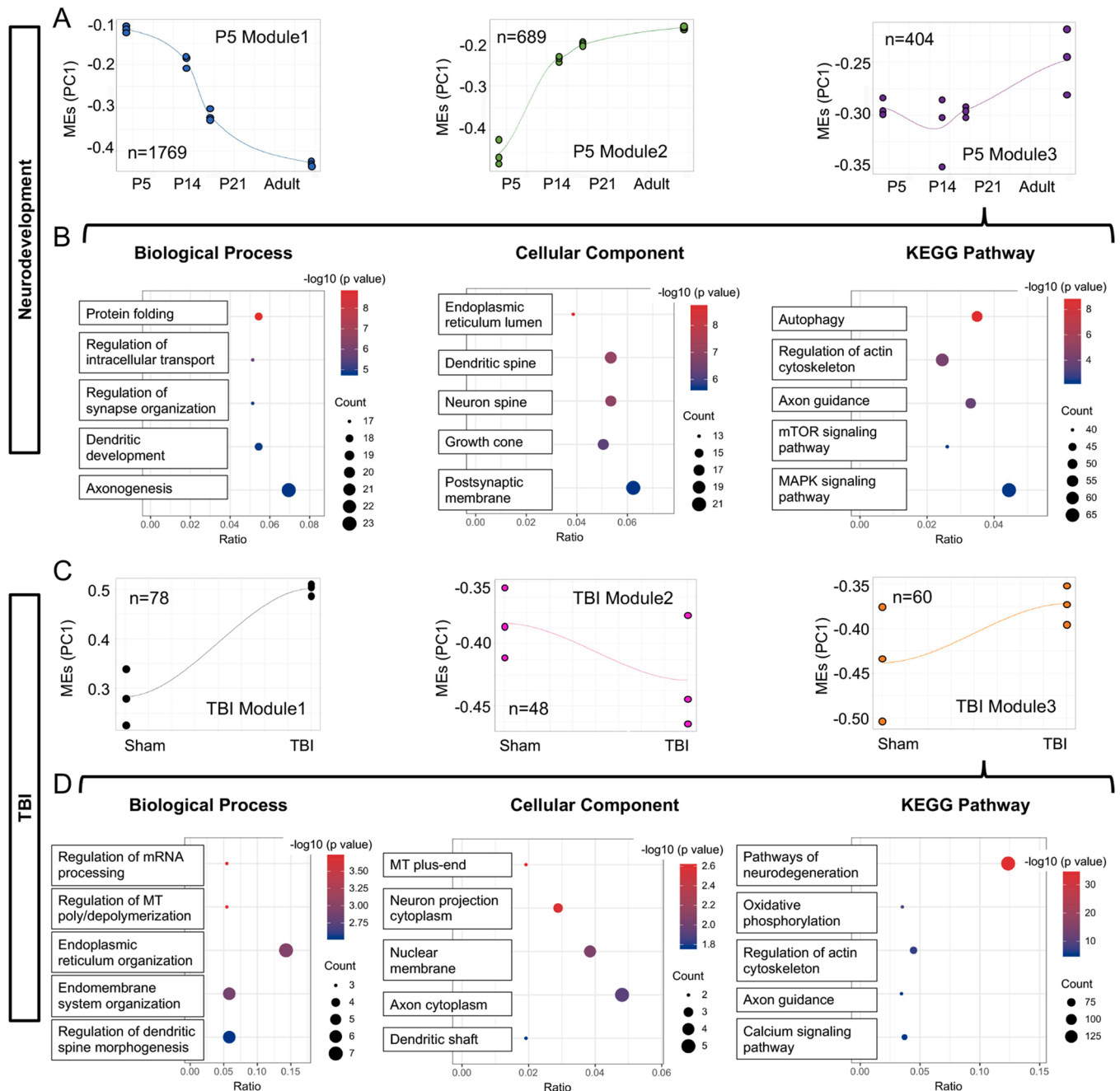
Fig. 5. Correlation analysis revealed modules related to development and TBI. (A) Weighted gene correlation network analysis (WGCNA) identified three significant protein modules associated with developmental stages. The total numbers of protein were listed in each module. Non-linear trajectories were represented as postnatal days (x-axis) relative to module eigengenes (MEs) expression (y-axis). (B) Enrichments of biological process, cellular components, and KEGG pathway were shown for P5 module 3 during development. (C-D) WGCNA identified another three significant protein modules associated with TBI and enrichments were shown for TBI module 3 related to axon.

axon growth, such as synaptogenesis signaling pathway, axonal guidance, regulation of eIF4/p70S6K and mTOR signaling, were also involved suggesting TBI may harnessing complex developmental programs.

4.2.2. Clustering of protein trajectories reveals waves of changes in association with axonal molecular control during development and after TBI

The relationship between proteome dynamics and development (particularly at P5) or TBI conditions were investigated using an unsupervised WGNCA analysis which clustered proteins with similar significant trajectories. Together, a total of 14 discrete modules (7 protein clusters in each dataset) were identified and 3 modules from each condition showed distinct correlation (Fig. 5 and Table S5). As expected, some of those modules were not directly related to changes in axon, but rather involved in other important biological processes. Specifically, during development, P5 module 1 (n = 1769 proteins, R=0.96) maintained biological processes of synaptic modulation and clustered within synaptic cellular components displaying a decreasing trend, indicative of synaptic pruning (Fig. S7A-B). P5 module 2 (n = 689 proteins, R=0.84) showed an increasing trend relevant to nuclear RNA and mRNA processing, implying of elevated protein translation during brain maturation (Fig. S7C-D). Nonetheless, P5 module 3 (n = 404 proteins,
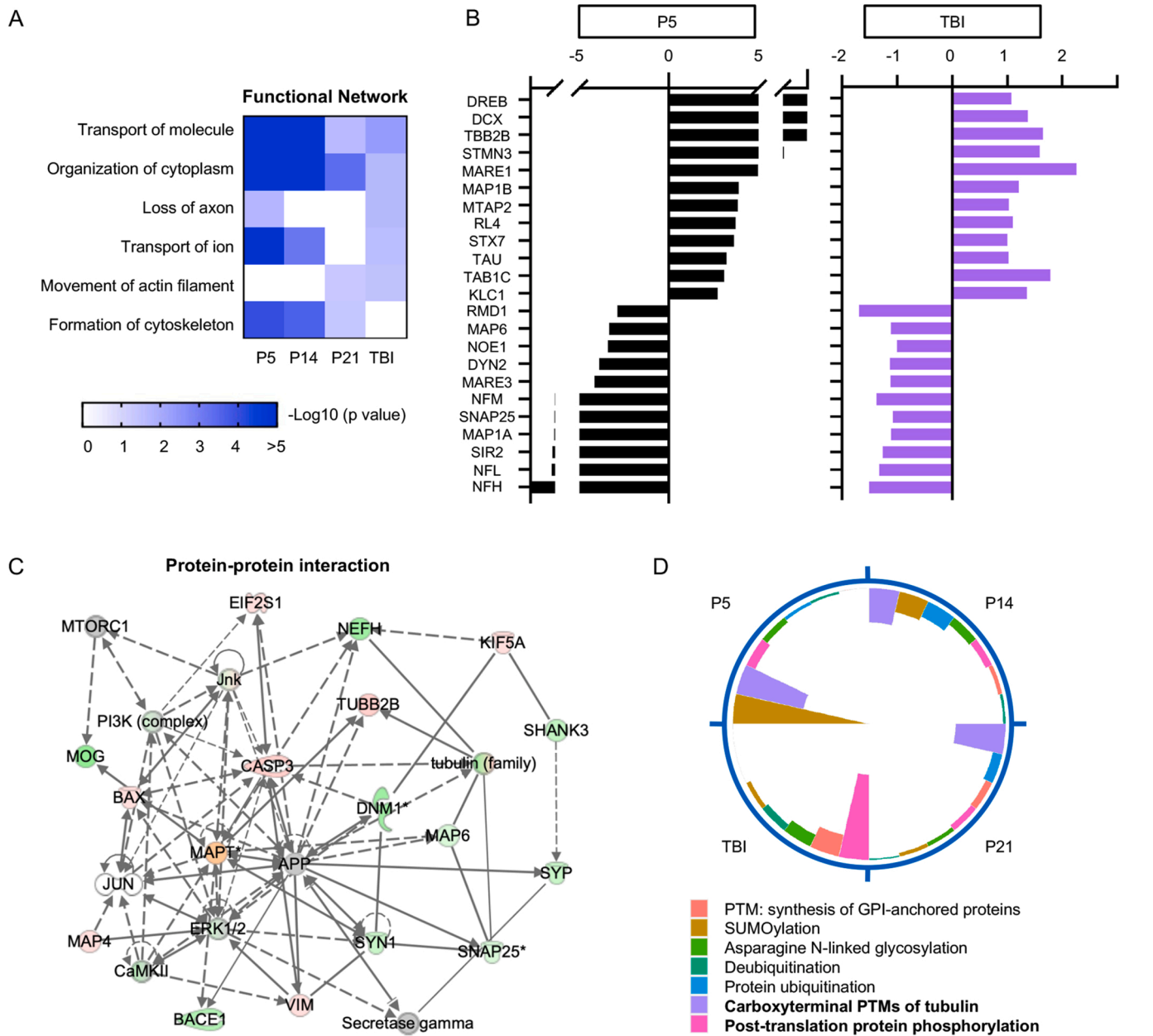
Fig. 6. Functional network, protein-protein interaction, and Reactome analysis highlighted axonal protein involvement during development and after TBI. (A) Functional networks revealed dynamic axon and cytoskeleton regulation during DAD and following TBI. (B) Relative expression changes of axonal proteins relevant to those networks were compared between P5 and TBI. (C) Interactions of relevant differentially expressed proteins was shown using IPA. Red and green colors coded proteins represented upregulation and downregulation, respectively. The degree of regulation was manifested by the color intensity. Solid lines in the network implied direct interactions between proteins, and dashed lines indicate indirect interactions. Geometric shapes represented different general functional families of gene regulation (standing oval for ion channel, flat oval for transcription regulator, trapezoid for transporter, three triangles for kinase, irregular for enzyme, deltoid with empty circle inside for peptidase, and circle for others). (D) Wind rose graph illustrated the list of specific PTMs pathways enriched in Reactome knowledgebase (R-RNO-597592). The color of each represented a single PTMs pathway. The height of the bar was based and ranked on the p value of each pathway.

R=0.62) was distinctively associated with axonal and cytoskeleton regulation (Fig. 5B and Table S6). Indeed, biological processes of module 3 were highly enriched with protein folding, regulation of intracellular transport, regulation of synapse organization, dendrite development, and axonogenesis. The main cellular components included endoplasmic reticulum lumen, dendritic spine, neuron spine, growth cone, and postsynaptic membrane. Interestingly, canonical pathway annotation revealed involvement of autophagy, regulation of actin cytoskeleton, axon guidance, mTOR signaling pathway, and MAPK signaling pathway that reflecting axon growth as well as DAD.

Similarly, three distinct modules were found correlated and explained the most variance for TBI outcomes (Fig. 5C). Specifically, TBI module 1 (n = 78 proteins, R=0.96), with an increasing trend, was related to biological process of reactive oxygen species metabolic process, regulation of protein modification, and amyloid fibril formation, with cellular component enrichments in synapse, cell cortex, and MT (Fig. S8A-B). TBI Module 2 (n = 48 proteins, R=0.59), with a decreasing trend, was associated with biological processes of regulation of transporter activity, RNA splicing, and synaptic vesicle endocytosis, with major cellular components of synapse, neurofilament, and mitochondrial outer membrane (Fig. S8C-D). Uniquely, TBI induced axon repair/degeneration molecular profiles were mostly reflected by TBI module 3 (n = 60 proteins, R=0.64) with top biological processes of regulation of mRNA processing, MT poly-/depolymerization, and dendritic spine morphogenesis (Table S6). Indeed, MT, axon cytoplasm, and dendritic shaft were the major cellular components involved. Pathway analysis further revealed enrichments of neurodegeneration, oxidative phosphorylation, regulation of actin cytoskeleton, axon guidance, and calcium signaling after TBI, reflecting complex programs for concurrent axon repair and degeneration (Fig. 5D). Together, similar protein trajectories associated with axon and cytoskeleton control during development and after TBI were delineated.

4.3. Development and TBI share similar molecular and functional networks

To provide a deeper understanding of the individual molecular annotation between development and TBI, functional networks were mapped and compared. Interestingly, molecular and ion transport, cytoplasm organization, and axonal loss were evidently shown especially at P5 and after TBI (Fig. 6A). In contrast, formation of cytoskeleton was distinct during development, reflecting a program towards axon growth. Similarly, movement of actin filament was only identified after TBI, suggesting changes more specific to TAI.

The network analysis provided additional insights by examining integrated protein expression changes. Within functional networks, differentially expressed proteins highlighted axon enrichments. Indeed, with an overall higher degree of protein fold changes during development, concurrent upregulations of MT associated proteins (tau (MAPT/TAU), EB1 (MARE1), MAP1B, MTAP2, doublecortin (DCX)), stathmin 3 (STMN3, MT-destabilizing), kinesin light chain 1 (KLC1), and tubulin (TBB2B and TBA1C) families of proteins were recapitulated after TBI (Fig. 6B and Table S7). Likewise, MT associated proteins (MAP6, EB3 (MARE3), regulator of MT dynamics protein 1 (RMD1)), neurofilament (NF-H/M/L), dynamin-2 (DYN2), and sirtuin 2 (SIR2, NAD-dependent protein deacetylase) proteins were downregulated both throughout development and after TBI.

Interaction of such differentially expressed protein profiles was found associated with cellular assembly and organization, cell-to-cell signaling and interaction, nervous system development and function, and neurological disease by IPA analysis (Fig. 6C). In particular, direct (solid) and indirect (dashed line) protein-protein interactions of tau, MAP6, caspase 3 (CASP3), APP, c-Jun (JUN), c-Jun N-terminal kinase (JNK), calcium/calmodulin dependent protein kinase II (CaMKII), ERK1/2, dynamin-1 (DNM1), neurofilament heavy (NEFH) (validated in Fig. S4A-B), and tubulin (family) were centralized, mostly implying

axon degeneration changes.

As another regulator of the proteome functions, post-translational modifications (PTMs) were found playing a key role modulating processes of axon growth/repair and degeneration (Fig. 6D and Table S8). Those PTM pathways (R-RNO-597592) included phosphorylation, carboxyterminal PTMs of tubulin, protein ubiquitination, deubiquitination, glycosylation, SUMOylation, and synthesis of GPI-anchored proteins. In particular, among those, carboxyterminal PTMs of tubulin was particularly relevant to changes of axons with TUBB2B and families of α-tubulin (TUBA1C, LOC100909441 (tubulin α chain), TUBA3A, TUBA3B, TUBA4A, TUBA8) involved. These results confirmed the findings that similar tubulin PTMs were found and played roles regulating developmental and TBI related changes of axon that potentially driving axons towards either growth/repair or degeneration.

5. Discussion

Here, we explored the possibility that TBI recapitulates certain developmental changes of axons that drive them to either survival or degeneration. Indeed, we found multiple shared changes in axonal MT through PTMs of tubulin and MAPs during both conditions, that were further supported by proteomics analysis. This suggests that developmental pathways controlling axon cytoskeleton integrity are re-activated after TBI and may govern the selection processes of directing axons towards either a growth/repair or degenerative phenotypes (Fig. 7). While we also found multiple differences in protein profiles and signaling pathways beyond MT modifications, the present comparison approach demonstrates how focused evaluation of developmental processes may provide insight into pathways initiated by TBI. Overall, these data indicate the intriguing possibilities about the common mechanisms between development and after TBI and support further investigation in this area.

The MT network and its stability in neuronal axons are known to facilitate morphological and functional processes particularly during embryonic development, such as axon guidance and intracellular trafficking. Such MT stability is found tightly controlled by tubulin PTMs (Janke and Magiera, 2020). Surprisingly, in this study, we first identified diverse tubulin PTMs changes that were not only found common, but also essential between developmental program and after TBI. In particular, we found that degenerating axons lost Aceytl-Tub and PolyGlu-Tub profiles, indicating less stable MTs, and became enriched with Tyr-Tub, which colocalized near and within APP+ axonal swellings after TAI. This suggests that tyrosination plays a role in MT disassembly preceding axon degeneration. This is supported by a previous study that found MTs assembled from purified Tyr-Tub are depolymerized more efficiently than others (Sirajuddin et al., 2014). Further, it has been demonstrated that the addition of exogenous MT stabilizers, such as taxanes, can result in reduced expression of Tyr-Tub (Baas and Ahmad, 2013). This MT instability involves the kinesin family transport machinery (Peris et al., 2009), which is also shown to be upregulated in our proteomic dataset (KLC1).

In the present study, only a subset of axons appeared to undergo degeneration for both TBI and development, while nearby axons demonstrated evidence of a maintenance or repair process via sustained Aceytl-Tub and PolyGlu-Tub expression. Intriguingly, previous studies showed that both Aceytl-Tub and PolyGlu-Tub labeled stabilized long-lived MTs and influencing MT assembly (Magiera and Janke, 2014). This further supports our observation that both acetylation and polyglutamylation may be critical for MT stabilization, thereby potentially permitting growth/repair. Together, these data indicate that PTMs play an important role in controlling MT behavior at molecular level, thus affecting both axon growth/repair and degeneration processes.

Besides tubulin PTMs, MT can also be regulated by interaction with MAPs, especially tau and MAP6 that are highly and selectively enriched in axons. Unique to the exceptionally thin and elongated architecture of axons, MTs are arranged in a unidirectional orientation with regular
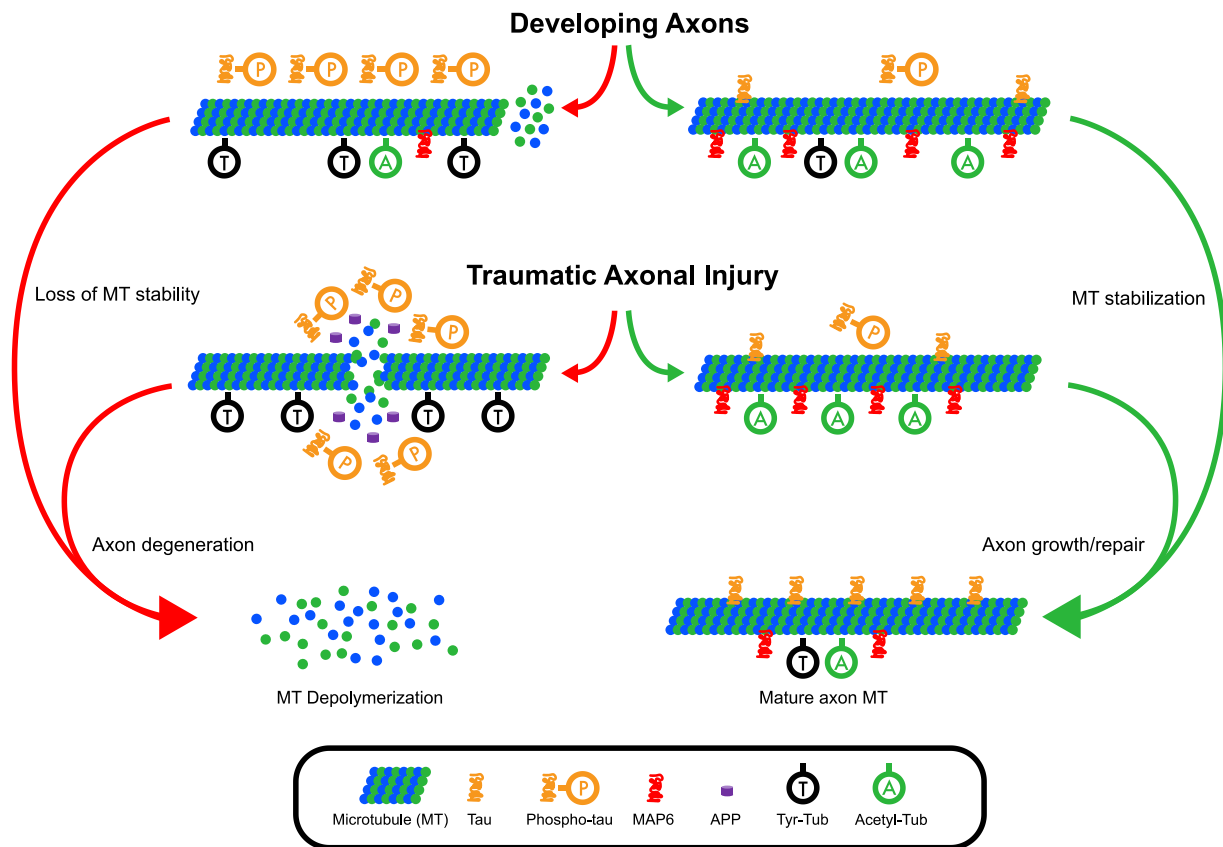
Fig. 7. Evolving axonal MT changes that are shared between development and TBI. For both development and TAI due to TBI, axons appear to be selected for one of two opposing pathways that lead to either loss or maintain of MT stability, therefore possibly leading to axon degeneration (red arrows) or growth/repair (green arrows). Changes in axonal MTs regulated by tubulin PTMs and MAPs may play a key role in defining each pathway. TAI induces MT damage and accumulation of APP. For both development and TBI, disconnection of tau from MTs and its subsequent phosphorylation is associated with loss of MT stabilization and axon degeneration. Conversely, enhanced MT stabilization with MAP6 supports MT stabilization and possibly determining axon growth/repair.

spacing. MAP6 and tau are thought to play important roles in stabilizing both individual MTs and the entire MT array within each axon via cross linking adjacent MTs. Here, we found evidence of increasing levels of total MAP6 during development, much in contrast to changes in total tau levels. Intriguingly, changes in MAP6 or alternatively, accumulation of p-tau occurred at the level of individual axons in the white matter. Indeed, early in development MAP6 is predominant (Bosc et al., 1996; Tortosa et al., 2017), and to a lesser extent by tau (Kempf et al., 1996). This is thought to reflect the need for much greater MT stabilization provided by MAP6 compared to tau as axons are being remodeled and elongated during development (Deloulme et al., 2015). Notably, depletion of tau in mature axons has been shown to result in an increase and broader distribution of MAP6, which was suggested to be a recapitulation of an developmental phenotype to compensate for loss of tau stabilization (Qiang et al., 2018). This enhanced stabilization may reflect an interplay between MAP6 and Acetyl-Tub (Deloulme et al., 2015). However, once axons are mature, tau becomes the dominant MAP, although the evolutionary reason for shifting to a more weakly stabilizing MAP remains unknown.

In contrast to development, we have recently shown that under dynamic stretch injury of axons in an in vitro model of TAI, high stress produced by tau at the MT binding sites can cause immediate mechanical rupture of the MTs (Ahmadzadeh et al., 2015). This leads to interruption of axonal transport, MT release of tau, phosphorylation of free tau, and accumulation of proteins, including p-tau in axonal swellings (Tang-Schomer et al., 2012), as has been shown after TBI in humans and in preclinical models, (Abu Hamdeh et al., 2018; Johnson et al., 2012; Uryu et al., 2007; Zanier et al., 2018). Phosphorylation of tau prevents its rebinding to MTs, resulting in additional MT instability that can

further drive axon degeneration.

In the present study, we found increases of axonal p-tau both during development and after TBI, albeit with a different expression pattern. Indeed, p-tau did not co-localized with DeTyr-Tub, which is a marker of stable MTs. Although the mechanism leading to phosphorylation and accumulation of tau in developing axons is unclear, its identification may represent a newfound marker of axon degeneration, similar to what has been described in TBI. However, unsurprisingly, more p-tau was found accumulating in axons after TBI than in development most likely due to far more frank axon transport interruption induced by the mechanical injury. The expression of p-tau in axons suggests compromised MT turnover, which may drive increasing MT destabilization, increased protein transport interruption and ultimately, degeneration. Indeed, p-tau in damaged axons has been hypothesized to be an initial event in the development of tau and amyloid-beta pathologies after TBI, including those found in chronic traumatic encephalopathy (Johnson et al., 2012; Smith et al., 2019).

As a potential inverse correlate to the expression of p-tau found in association with axon degeneration, we found that increased expression of MAP6 exclusively appeared in axons that did not have swellings or any indication of degeneration. Interestingly, these increases in MAP6 were co-localized with Acetyl-Tub but not Try-Tub. This supports a possible scenario that an endogenous axon repair mechanism is induced by trauma, whereby MAP6 replaces detached tau leading to enhanced MT stabilization (Bodakuntla et al., 2019). This is also corroborated by a previous in vitro study of TAI, where application of strongly stabilizing taxanes that bind to the tau binding domains on MTs prevented loss of MTs, which was associated with substantially reduces axon degeneration (Tang-Schomer et al., 2010).

Conversely, a loss of MAP6 after TBI was observed in degenerating axons with profound transport interruption. This finding is consistent with an in vitro study showing that MAP6 knock-down leads to increased varicosities generated under mechanical deformation (Gu et al., 2017). Importantly, reduction of MAP6 often leads to neurobehavioral changes, including reduced activity and deficits in social interactions, that is associated with impaired axon fiber integrity (Volle et al., 2013). Collectively, these observations suggest that increased MAP6 promotes axon growth/repair, while decreased MAP6 may pushes axon towards degeneration.

While omics have widely been used to understand brain development (Poulopoulos et al., 2019) and the concept of molecular interplay between axon degeneration and regeneration has been broadly discussed (Girouard et al., 2018), there has been limited identification of molecular changes associated with development and scant comparisons with TBI (Sowers et al., 2018). Here, we provide its direct comparison in brain proteome. Interestingly, by coupling proteome analysis from both processes, proteins with axon enrichments were found differentially expressed in similar trajectories and functional networks. These proteome changes led to the identification of common pathways related to axon degeneration, such as oxidative phosphorylation and MAPK signaling, implicated both during DAD and after TBI. Indeed, oxidative phosphorylation triggers axon degradation through Sarm1 (Summers et al., 2014), and MAPK promotes axon degeneration by facilitating the turnover of NMNAT2 (an NAD$^+$ biosynthetic enzyme for axon maintenance) (Walker et al., 2017). Surprisingly, several shared pathways of axon growth, including axon guidance as well as eIF4/p70S6K and mTOR signaling (involved in building axons and maturing tracts (Poulopoulos et al., 2019; Takei and Nawa, 2014)), were also recaptured after TBI. In particular, mTOR and phosphorylation of eIF4/S6K were found controlling localized axonal mRNA translation and protein synthesis (Jung et al., 2012). This indicates that axon growth mechanisms during development may be utilized for repair after injury, in part through active axonal protein turnover.

Looking into the upstream regulators of those signaling pathways, we further find distinct transcription factor involvements in each processes. Specifically, development not only needs maf as shown before (Nord et al., 2015), but also appears to require sirtuin 2 and shank3 for regulating tubulin and cytoskeleton changes. In contrast, TBI potentially induces a more robust gene response in related to histone modifications by histone h4 and CREBBP. Together, these results highlight a complicated scheme, where programs selecting for axon growth and loss during development occur concurrently. These overlapping processes appear to be reawakened after TBI to repair axonal structure in salvageable axons and clear axons that are too damaged.

Notably, although the present data uncovers many similarities in axon changes between development and TBI, substantial differences in protein profiles and signaling pathways were also found. For example, EIF2 and CREB signaling in neurons pathways are highly enriched in development, whereas SAPK/JNK signaling, Nrf2-mediated oxidative stress response, and pathways of neurodegeneration are involved after TBI. Further, protein module analysis reflected distinct biological processes of RNA and neurotransmitter activities during development, as opposed to protein misfolding and reactive oxygen species processes after TBI. These differences are expected at the whole brain level as developing brain involves complex physiological adaptation while TBI often set a series of pathological cascades related to immediate mechanical damage. Nevertheless, as fitting within the scope of this study, we specifically focus on the common axon-related proteome and associated pathways to provide new insights into axon growth/repair and degeneration.

Limitations in this study will be carefully addressed in future efforts. For example, the proteome data are shown in the context of mixed cellular components and cell types combining rat cortex and subcortical white matter. Although there was general agreement with histological findings of changes in axons, the results from tissue extracts may not be

specific to axons and could reflect changes in other neuronal compartments or other cell populations. It also worth noting that the proteome changes and bioinformatics analysis performed here reflects a series of global brain events far beyond axon growth/repair or degeneration. While the current data suggests the intriguing possibilities about common mechanisms between development and after TBI, further experimentation is required to examine the observed associations. Therefore, future in vitro studies may better parse specific axonal pathways. In addition, with the recent observations that female athletes participating in the same sport as males have a higher rate of concussion and worse outcomes and that female and male axons respond differently to the same mechanical trauma (Bretzin et al., 2021), potential sex differences in axon degeneration and repair after TBI should be considered (Dolle et al., 2018). Finally, with the recognition that progressive axon degeneration can continue for many years after TBI, an expanded temporal evaluation of evolving molecular processes of axon repair and degeneration is warranted (Johnson et al., 2013). This is especially important considering that progressive axon degeneration is thought to be a key process in the chronic and progressive TBI-related neurodegeneration (Johnson et al., 2017).

Taken together, the current data suggests that TBI recapitulates many developmental processes related to axon degeneration and growth, especially regarding MT dynamics. Specifically, the immediate mechanical damage to the axonal ultrastructure due to TBI appears to trigger a developmental selection process that drives some axons towards repair/recovery and others towards degeneration. These hypothesis-driving observations support further examinations of potential mechanistic links of axon fate between development and TBI that could reveal therapeutic targets to promote axon recovery and mitigate axon degeneration.

CRediT authorship contribution statement

Hailong Song: Conceptualization, Methodology, Investigation, Visualization, Writing - original draft, Writing - review & editing. **Chen Chen:** Methodology, Investigation, Visualization. **Brian Kelley:** Methodology, Investigation. **Alexandra Tomasevich:** Investigation. **Hyoungjoo Lee:** Methodology. **Jean-Pierre Dolle:** Conceptualization, Writing - review & editing. **Jianlin Cheng:** Methodology, Visualization. **Benjamin Garcia:** Methodology. **David F. Meaney:** Investigation, Writing - review & editing. **Douglas H. Smith:** Conceptualization, Investigation, Writing – original draft, Writing – review & editing.

Competing interests

None.

data collection and analysis, decision to publish, or preparation of the manuscript.

Appendix A. Supporting information

Supplementary data associated with this article can be found in the online version at doi:10.1016/j.pneurobio.2022.102332.

References

Abu Hamdeh, S., Shevchenko, G., Mi, J., Musunuri, S., Bergquist, J., Marklund, N., 2018. Proteomic differences between focal and diffuse traumatic brain injury in human brain tissue. Sci. Rep. 8, 6807.

Ahmadzadeh, H., Smith, D.H., Shenoy, V.B., 2015. Mechanical effects of dynamic binding between tau proteins on microtubules during axonal injury. Biophys. J. 109, 2328–2337.

Baas, P.W., Ahmad, F.J., 2013. Beyond taxol: microtubule-based treatment of disease and injury of the nervous system. Brain 136, 2937–2951.

Baas, P.W., Rao, A.N., Matamoros, A.J., Leo, L., 2016. Stability properties of neuronal microtubules. Cytoskeleton 73, 442–460.

Bagri, A., Cheng, H.J., Yaron, A., Pleasure, S.J., Tessier-Lavigne, M., 2003. Stereotyped pruning of long hippocampal axon branches triggered by retraction inducers of the semaphorin family. Cell 113, 285–299.

Bai, B., Wang, X., Li, Y., Chen, P.C., Yu, K., Dey, K.K., Yarbro, J.M., Han, X., Lutz, B.M., Rao, S., Jiao, Y., Sifford, J.M., Han, J., Wang, M., Tan, H., Shaw, T.I., Cho, J.H., Zhou, S., Wang, H., Niu, M., Mancieri, A., Messler, K.A., Sun, X., Wu, Z., Pagala, V., High, A.A., Bi, W., Zhang, H., Chi, H., Haroutunian, V., Zhang, B., Beach, T.G., Yu, G., Peng, J., 2020. Deep multilayer brain proteomics identifies molecular networks in Alzheimer's disease progression. Neuron 105 (975–991), e977.

Bodakuntla, S., Jijumon, A.S., Villablanca, C., Gonzalez-Billault, C., Janke, C., 2019. Microtubule-associated proteins: structuring the cytoskeleton. Trends Cell Biol. 29, 804–819.

Bosc, C., Cronk, J.D., Pirollet, F., Watterson, D.M., Haiech, J., Job, D., Margolis, R.L., 1996. Cloning, expression, and properties of the microtubule-stabilizing protein STOP. Proc. Natl. Acad. Sci. USA 93, 2125–2130.

Bramlett, H.M., Kraydieh, S., Green, E.J., Dietrich, W.D., 1997. Temporal and regional patterns of axonal damage following traumatic brain injury: a beta-amyloid precursor protein immunocytochemical study in rats. J. Neuropathol. Exp. Neurol. 56, 1132–1141.

Bretzin, A.C., Covassin, T., Wiebe, D.J., Stewart, W., 2021. Association of sex with adolescent soccer concussion incidence and characteristics. JAMA Netw. Open 4, e218191.

Cagnetta, R., Wong, H.H., Frese, C.K., Mallucci, G.R., Krijgsveld, J., Holt, C.E., 2019. Noncanonical modulation of the eIF2 pathway controls an increase in local translation during neural wiring. Mol. Cell 73 (474–489), e475.

Clausen, F., Hillered, L., Marklund, N., 2019. The fluid percussion injury rodent model in preclinical research on traumatic brain injury. In: Risling, M., Davidsson, J. (Eds.), Animal Models of Neurotrauma. Springer New York, New York, NY, pp. 3–18.

Cowan, W.M., Fawcett, J.W., O'Leary, D.D., Stanfield, B.B., 1984. Regressive events in neurogenesis. Science 225, 1258–1265.

Deloulme, J.C., Gory-Faure, S., Mauconduit, F., Chauvet, S., Jonckheere, J., Boulan, B., Mire, E., Xue, J., Jany, M., Maucler, C., Deparis, A.A., Montigon, O., Daoust, A., Barbier, E.L., Bosc, C., Deglon, N., Brocard, J., Denarier, E., Le Brun, I., Pernet-Gallay, K., Vilgrain, I., Robinson, P.J., Lahrech, H., Mann, F., Andrieux, A., 2015. Microtubule-associated protein 6 mediates neuronal connectivity through Semaphorin 3E-dependent signalling for axonal growth. Nat. Commun. 6, 7246.

Dolle, J.P., Jaye, A., Anderson, S.A., Ahmadzadeh, H., Shenoy, V.B., Smith, D.H., 2018. Newfound sex differences in axonal structure underlie differential outcomes from in vitro traumatic axonal injury. Exp. Neurol. 300, 121–134.

Gentleman, S.M., Nash, M.J., Sweeting, C.J., Graham, D.I., Roberts, G.W., 1993. Beta-amyloid precursor protein (beta APP) as a marker for axonal injury after head injury. Neurosci. Lett. 160, 139–144.

Girouard, M.P., Bueno, M., Julian, V., Drake, S., Byrne, A.B., Fournier, A.E., 2018. The molecular interplay between axon degeneration and regeneration. Dev. Neurobiol. 78, 978–990.

Gu, Y., Jukkola, P., Wang, Q., Esparza, T., Zhao, Y., Brody, D., Gu, C., 2017. Polarity of varicosity initiation in central neuron mechanosensation. J. Cell Biol. 216, 2179–2199.

HaileMariam, M., Eguez, R.V., Singh, H., Bekele, S., Ameni, G., Pieper, R., Yu, Y., 2018. S-trap, an ultrafast sample-preparation approach for shotgun proteomics. J. Proteome Res 17, 2917–2924.

Hall, A., Lalli, G., 2010. Rho and ras GTPases in axon growth, guidance, and branching. Cold Spring Harb. Perspect. Biol. 2, a001818.

Hoopfer, E.D., McLaughlin, T., Watts, R.J., Schuldiner, O., O'Leary, D.D., Luo, L., 2006. Wlds protection distinguishes axon degeneration following injury from naturally occurring developmental pruning. Neuron 50, 883–895.

Janke, C., Magiera, M.M., 2020. The tubulin code and its role in controlling microtubule properties and functions. Nat. Rev. Mol. Cell Biol. 21, 307–326.

Johnson, V.E., Stewart, W., Arena, J.D., Smith, D.H., 2017. Traumatic brain injury as a trigger of neurodegeneration. Adv. Neurobiol. 15, 383–400.

Johnson, V.E., Stewart, W., Smith, D.H., 2012. Widespread tau and amyloid-beta pathology many years after a single traumatic brain injury in humans. Brain Pathol. 22, 142–149.

Johnson, V.E., Stewart, W., Smith, D.H., 2013. Axonal pathology in traumatic brain injury. Exp. Neurol. 246, 35–43.

Johnson, V.E., Stewart, W., Weber, M.T., Cullen, D.K., Siman, R., Smith, D.H., 2016. SNTF immunostaining reveals previously undetected axonal pathology in traumatic brain injury. Acta Neuropathol. 131, 115–135.

Jung, H., Yoon, B.C., Holt, C.E., 2012. Axonal mRNA localization and local protein synthesis in nervous system assembly, maintenance and repair. Nat. Rev. Neurosci. 13, 308–324.

Kempf, M., Clement, A., Faissner, A., Lee, G., Brandt, R., 1996. Tau binds to the distal axon early in development of polarity in a microtubule- and microfilament-dependent manner. J. Neurosci. 16, 5583–5592.

Koch, P.F., Cottone, C., Adam, C.D., Ulyanova, A.V., Russo, R.J., Weber, M.T., Arena, J. D., Johnson, V.E., Wolf, J.A., 2020. Traumatic brain injury preserves firing rates but disrupts laminar oscillatory coupling and neuronal entrainment in hippocampal CA1. eNeuro 7.

Langfelder, P., Horvath, S., 2008. WGCNA: an R package for weighted correlation network analysis. BMC Bioinform. 9, 559.

Li, X.H., Chen, C., Tu, Y., Sun, H.T., Zhao, M.L., Cheng, S.X., Qu, Y., Zhang, S., 2013. Sirt1 promotes axonogenesis by deacetylation of Akt and inactivation of GSK3. Mol. Neurobiol. 48, 490–499.

Li, Y., Chopp, M., Chen, J., Wang, L., Gautam, S.C., Xu, Y.X., Zhang, Z., 2000. Intrastriatal transplantation of bone marrow nonhematopoietic cells improves functional recovery after stroke in adult mice. J. Cereb. Blood Flow Metab. 20, 1311–1319.

Luo, L., O'Leary, D.D., 2005. Axon retraction and degeneration in development and disease. Annu. Rev. Neurosci. 28, 127–156.

Magiera, M.M., Janke, C., 2014. Post-translational modifications of tubulin. Curr. Biol. 24, R351–R354.

Moutin, M.J., Bosc, C., Peris, L., Andrieux, A., 2021. Tubulin post-translational modifications control neuronal development and functions. Dev. Neurobiol. 81, 253–272.

Nord, A.S., Pattabiraman, K., Visel, A., Rubenstein, J.L.R., 2015. Genomic perspectives of transcriptional regulation in forebrain development. Neuron 85, 27–47.

O'Leary, D.D., Stanfield, B.B., Cowan, W.M., 1981. Evidence that the early postnatal restriction of the cells of origin of the callosal projection is due to the elimination of axonal collaterals rather than to the death of neurons. Brain Res. 227, 607–617.

Peris, L., Wagenbach, M., Lafanechere, L., Brocard, J., Moore, A.T., Kozielski, F., Job, D., Wordeman, L., Andrieux, A., 2009. Motor-dependent microtubule disassembly driven by tubulin tyrosination. J. Cell Biol. 185, 1159–1166.

Pernici, C.D., Rowe, R.K., Doughty, P.T., Madadi, M., Lifshitz, J., Murray, T.A., 2020. Longitudinal optical imaging technique to visualize progressive axonal damage after brain injury in mice reveals responses to different minocycline treatments. Sci. Rep. 10, 7815.

Pierce, J.E., Trojanowski, J.Q., Graham, D.I., Smith, D.H., McIntosh, T.K., 1996. Immunohistochemical characterization of alterations in the distribution of amyloid precursor proteins and beta-amyloid peptide after experimental brain injury in the rat. J. Neurosci. 16, 1083–1090.

Poulopoulos, A., Murphy, A.J., Ozkan, A., Davis, P., Hatch, J., Kirchner, R., Macklis, J.D., 2019. Subcellular transcriptomes and proteomes of developing axon projections in the cerebral cortex. Nature 565, 356–360.

Povlishock, J.T., Christman, C.W., 1995. The pathobiology of traumatically induced axonal injury in animals and humans: a review of current thoughts. J. Neurotrauma 12, 555–564.

Purohit, P.K., Smith, D.H., 2016. A model for stretch growth of neurons. J. Biomech. 49, 3934–3942.

Qiang, L., Sun, X., Austin, T.O., Muralidharan, H., Jean, D.C., Liu, M., Yu, W., Baas, P.W., 2018. Tau does not stabilize axonal microtubules but rather enables them to have long labile domains. Curr. Biol. 28 (2181–2189), e2184.

Sampaio-Baptista, C., Johansen-Berg, H., 2017. White matter plasticity in the adult brain. Neuron 96, 1239–1251.

Schweitzer, J.B., Park, M.R., Einhaus, S.L., Robertson, J.T., 1993. Ubiquitin marks the reactive swellings of diffuse axonal injury. Acta Neuropathol. 85, 503–507.

Searle, B.C., Pino, L.K., Egertson, J.D., Ting, Y.S., Lawrence, R.T., MacLean, B.X., Villen, J., MacCoss, M.J., 2018. Chromatogram libraries improve peptide detection and quantification by data independent acquisition mass spectrometry. Nat. Commun. 9, 5128.

Sirajuddin, M., Rice, L.M., Vale, R.D., 2014. Regulation of microtubule motors by tubulin isotypes and post-translational modifications. Nat. Cell Biol. 16, 335–344.

Smith, D.H., 2009. Stretch growth of integrated axon tracts: extremes and exploitations. Prog. Neurobiol. 89, 231–239.

Smith, D.H., Chen, X.H., Pierce, J.E., Wolf, J.A., Trojanowski, J.Q., Graham, D.I., McIntosh, T.K., 1997. Progressive atrophy and neuron death for one year following brain trauma in the rat. J. Neurotrauma 14, 715–727.

Smith, D.H., Johnson, V.E., Trojanowski, J.Q., Stewart, W., 2019. Chronic traumatic encephalopathy - confusion and controversies. Nat. Rev. Neurol. 15, 179–183.

Smith, D.H., Meaney, D.F., 2000. Axonal damage in traumatic brain injury. Neuroscientist 6, 483–495.

Smith, D.H., Stewart, W., 2020. 'Concussion' is not a true diagnosis. Nat. Rev. Neurol. 16, 457–458.

Smith, G.M., Gallo, G., 2018. The role of mitochondria in axon development and regeneration. Dev. Neurobiol. 78, 221–237.

Song, H., Chen, M., Chen, C., Cui, J., Johnson, C.E., Cheng, J., Wang, X., Swerdlow, R.H., DePalma, R.G., Xia, W., Gu, Z., 2019a. Proteomic analysis and biochemical correlates of mitochondrial dysfunction after low-intensity primary blast exposure. J. Neurotrauma 36, 1591–1605.

Song, H., Zhou, H., Qu, Z., Hou, J., Chen, W., Cai, W., Cheng, Q., Chuang, D.Y., Chen, S., Li, S., Li, J., Cheng, J., Greenlief, C.M., Lu, Y., Simonyi, A., Sun, G.Y., Wu, C., Cui, J., Gu, Z., 2019b. From analysis of ischemic mouse brain proteome to identification of human serum clusterin as a potential biomarker for severity of acute ischemic stroke. Transl. Stroke Res. 10, 546–556.

Song, Y., Brady, S.T., 2015. Post-translational modifications of tubulin: pathways to functional diversity of microtubules. Trends Cell Biol. 25, 125–136.

Sowers, J.L., Wu, P., Zhang, K., DeWitt, D.S., Prough, D.S., 2018. Proteomic changes in traumatic brain injury: experimental approaches. Curr. Opin. Neurol. 31, 709–717.

Stanfield, B.B., O'Leary, D.D., Fricks, C., 1982. Selective collateral elimination in early postnatal development restricts cortical distribution of rat pyramidal tract neurones. Nature 298, 371–373.

Summers, D.W., DiAntonio, A., Milbrandt, J., 2014. Mitochondrial dysfunction induces Sarm1-dependent cell death in sensory neurons. J. Neurosci. 34, 9338–9350.

Takei, N., Nawa, H., 2014. mTOR signaling and its roles in normal and abnormal brain development. Front. Mol. Neurosci. 7, 28.

Tang-Schomer, M.D., Johnson, V.E., Baas, P.W., Stewart, W., Smith, D.H., 2012. Partial interruption of axonal transport due to microtubule breakage accounts for the formation of periodic varicosities after traumatic axonal injury. Exp. Neurol. 233, 364–372.

Tang-Schomer, M.D., Patel, A.R., Baas, P.W., Smith, D.H., 2010. Mechanical breaking of microtubules in axons during dynamic stretch injury underlies delayed elasticity, microtubule disassembly, and axon degeneration. FASEB J. 24, 1401–1410.

The Gene Ontology, C., 2019. The Gene Ontology Resource: 20 years and still GOing strong. Nucleic Acids Res. 47, D330–D338.

Tortosa, E., Adolfs, Y., Fukata, M., Pasterkamp, R.J., Kapitein, L.C., Hoogenraad, C.C., 2017. Dynamic palmitoylation targets MAP6 to the axon to promote microtubule stabilization during neuronal polarization. Neuron 94 (809–825), e807.

Uryu, K., Chen, X.H., Martinez, D., Browne, K.D., Johnson, V.E., Graham, D.I., Lee, V.M., Trojanowski, J.Q., Smith, D.H., 2007. Multiple proteins implicated in neurodegenerative diseases accumulate in axons after brain trauma in humans. Exp. Neurol. 208, 185–192.

Volle, J., Brocard, J., Saoud, M., Gory-Faure, S., Brunelin, J., Andrieux, A., Suaud-Chagny, M.F., 2013. Reduced expression of STOP/MAP6 in mice leads to cognitive deficits. Schizophr. Bull. 39, 969–978.

Walker, L.J., Summers, D.W., Sasaki, Y., Brace, E.J., Milbrandt, J., DiAntonio, A., 2017. MAPK signaling promotes axonal degeneration by speeding the turnover of the axonal maintenance factor NMNAT2. Elife 6.

Watts, R.J., Hoopfer, E.D., Luo, L., 2003. Axon pruning during Drosophila metamorphosis: evidence for local degeneration and requirement of the ubiquitin-proteasome system. Neuron 38, 871–885.

Yang, J., Weimer, R.M., Kallop, D., Olsen, O., Wu, Z., Renier, N., Uryu, K., Tessier-Lavigne, M., 2013. Regulation of axon degeneration after injury and in development by the endogenous calpain inhibitor calpastatin. Neuron 80, 1175–1189.

Zanier, E.R., Bertani, I., Sammali, E., Pischiutta, F., Chiaravalloti, M.A., Vegliante, G., Masone, A., Corbelli, A., Smith, D.H., Menon, D.K., Stocchetti, N., Fiordaliso, F., De Simoni, M.G., Stewart, W., Chiesa, R., 2018. Induction of a transmissible tau pathology by traumatic brain injury. Brain 141, 2685–2699.